第 35 卷第 10 期 无 机 化 学 学 报 Vol.35 No.10
2019 年 10 月 CHINESE JOURNAL OF INORGANIC CHEMISTRY 1877-1884

基于双(苯并咪唑)桥联配体构筑的三个配位聚合物的合成、晶体结构及荧光识别性能

牛宇岚*,[1] 翟丽军[1] 郝小艳[1] 贾焦焦[1] 范黎明*,[1,2]
([1]太原工业学院化学与化工系,太原 030008)
([2]中北大学理学院,太原 030051)

摘要:利用双(苯并咪唑)桥联配体 1,4-双(2-苯并咪唑基)苯(bbib)和 4,4′-双(2-苯并咪唑基)联苯(bbibp)与过渡金属盐在水热条件下反应,合成了 3 种新型的一维配位聚合物,$\{[Mn(bbib)(H_2O)_4](H_2BTC)\cdot 2H_2O\}_n$ (**1**),$[Zn(bbib)Cl_2]_n$ (**2**)和$[Zn(bbibp)Cl_2]_n$ (**3**),并通过元素分析、红外光谱、粉末 X 射线衍射分析、单晶 X 射线衍射等对其结构进行了表征。结构分析表明,配合物 **1** 中的 O–H···O 氢键以及配合物 **2** 和 **3** 中的 C–H···Cl 氢键在上述配合物的三维超分子结构的构筑过程中起着重要的作用。在考虑配合物强氢键作用的基础上,配合物 **1** 的超分子结构可以简化为(4,6)-连接的$\{4^2\cdot 5^8\cdot 6^4\cdot 7\}\{4^2\cdot 6^4\}$网络,配合物 **2** 可以看做是一个 5-连接的$\{4^3\cdot 6^7\}$骨架,配合物 **3** 可以简化成 6-连接$(4^8\cdot 6^7)$-msw 网络结构。此外,荧光识别性能研究表明配合物 **2** 和 **3** 可以实现对水相中 Fe^{3+}离子的高灵敏性和高选择性识别。

关键词:配位聚合物;双(苯并咪唑)配体;晶体结构;荧光识别
中图分类号:O614.71+1;O614.24+1 **文献标识码**:A **文章编号**:1001-4861(2019)10-1877-08
DOI:10.11862/CJIC.2019.217

Syntheses, Crystal Structures, and Luminescence Sensing of Three Coordination Polymers Based on Bis(benzimidazole) Bridging Linkers

NIU Yu-Lan*,[1] ZHAI Li-Jun[1] HAO Xiao-Yan[1] JIA Jiao-Jiao[1] FAN Li-Ming*,[1,2]
([1]*Department of Chemistry and Chemical Engineering, Taiyuan Institute of Technology, Taiyuan* 030008, *China*)
([2]*Department of Chemistry, College of Science, North University of China, Taiyuan* 030051, *China*)

Abstract: Three 1D coordination polymers (CPs), namely, $\{[Mn(bbib)(H_2O)_4](H_2BTC)\cdot 2H_2O\}_n$ (**1**), $[Zn(bbib)Cl_2]_n$ (**2**), and $[Zn(bbibp)Cl_2]_n$ (**3**), have been assembled from the reaction of bbib (1,4-bis(2-benzimidazolyl)benzene) or bbibp (4,4′-bis(2-benzimidazolyl)biphenyl) and transition metal salts. Their structures have been determined by single-crystal X-ray diffraction analyses and further characterized by elemental analyses (EA), IR spectra, powder X-ray diffraction (PXRD), and thermogravimetric (TG) analyses. Structural analysis reveals that the strong O–H···O hydrogen bonds in **1**, and C–H···Cl hydrogen bonds in **2** and **3** play important roles in the formation of those CPs, with the final packing architectures being (4,6)-connected $\{4^2\cdot 5^8\cdot 6^4\cdot 7\}\{4^2\cdot 6^4\}$ net for **1**, 5-connected $\{4^3\cdot 6^7\}$ net for **2**, and 6-connected $(4^8\cdot 6^7)$-msw net for **3**. Besides, the luminescent sensing investigation indicates that complexes **2** and **3** exhibit highly sensitivity and selectively sensing of Fe^{3+} ion in aqueous solutions. CCDC: 1917435, **1**; 1917436, **2**; 1917437, **3**.

Keywords: coordination polymers; bis(benzimidazo-1-ly) ligand; crystal structure; luminescent sensing

收稿日期:2019-06-14。收修改稿日期:2019-07-21。
国家自然科学基金(No.21801230)和山西省自然科学基金(No.201801D221084)资助项目。
*通信联系人。E-mail:niuyulan@163.com,limingfan@nuc.edu.cn

0 Introduction

The coordination polymers (CPs), generally constructed from the organic linkers and the metal ions, have drawn more and more attentions for their potential applications in so many fields, such as gas separation, proton conduction, chemical sensing, ion exchange, and heterogeneous catalysis[1-5]. CPs have been widely implemented to a large extent within inorganic-organic hybrid materials for a number of years. However, the design of such materials with desired structural features and physicochemical properties are remain a challenge for not only the nature of the organic ligands but also the reaction conditions having great effects on the final architectures[6-8].

The rational selection of organic linkers seems an effective way to build CPs with desired structures. Among the numerous organic ligands, the N-donor linkers are favored for their stable backbones as well as the strong coordinating abilities, which can be act as bridging linkers, tripodal, or even tetrahedral shaped brackets in the formation of CPs[9-12]. In principle, the N-donors are electroneutral, when they coordinate with metal ions, the anions must be introduced to balance the charges. The anions can be common anions, such as the halogen ions, nitrate, sulfate, phosphate, acetate, oxalate, or even deprotonated polycarboxylates[13-15]. Numerous samples have proved that the bridged anions can expanded the dimensions, and the monodentate halogen ions can form strong hydrogen bonds[16-18].

Thus, these considerations inspired us to explore new coordination networks with bis (benzimidazole) linkers (Scheme 1) and transition metal salts under solvothermal conditions. Herein, we reported the syntheses and characterizations of three 1D CPs: {[Mn (bbib) $(H_2O)_4$] $(H_2BTC)\cdot 2H_2O\}_n$ (**1**), $[Zn(bbib)Cl_2]_n$ (**2**), and $[Zn(bbibp)Cl_2]_n$ (**3**). Structural analysis revealed that the strong O–H···O hydrogen bonds in **1**, and C–H ··· Cl hydrogen bonds in **2** and **3** play important roles in the formation of 3D structures of these CPs, with the final packing architectures being (4,6)-connected $\{4^2\cdot5^8\cdot6^4\cdot7\}\{4^2\cdot6^4\}$ net for **1**, 5-connected $\{4^3\cdot6^7\}$ net for **2**, and 6-connected $(4^8\cdot6^7)$-msw net for **3**, respectively. Besides, the luminescent sensing of complex **2** and **3** have been investigated.

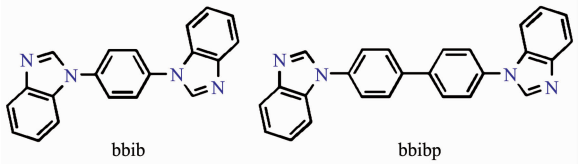

Scheme 1 Structures of two bis(benzimidazole) linkers

1 Experimental

1.1 Materials and methods

All the chemical reagents were purchased from Jinan Henghua Sci. & Technol. Co. Ltd. without further purification. IR spectra were measured on a NEXUS 670 FTIR spectrometer. Elemental analyses were carried out on a CE instruments EA 1110 elemental analyzer. Thermogravimetric analyses (TGA) were performed under N_2 atmosphere with the heating rate of 10 ℃·min^{-1} on PerkinElmer DTA6000 thermogravimetric analyzer. X-ray powder diffractions were measured on a Panalytical X-Pert pro diffractometer (D/max 2500PC, Rigaku) at 50 kV, 30 mA by using Cu $K\alpha$ radiation (λ=0.154 06 nm) with 2θ range from 5° to 50°. Fluorescent data were collected on Hitachi F-7000 FL Spectrophotometer. UV-Vis spectra were collected on the Hitachi U-3500 UV-Vis spectrometer.

1.2 Synthesis

1.2.1 Synthesis of $\{[Mn(bbib)(H_2O)_4](H_2BTC)\cdot 2H_2O\}_n$ (**1**)

A mixture of H_4BTC (0.10 mmol, 0.025 g), bbib (0.20 mmol, 0.062 g), $MnSO_4\cdot H_2O$ (0.20 mmol, 0.034 g) was put into 6 mL H_2O and then transferred to a 25 mL Teflon-lined stainless steel vessel, heated at 110 ℃ for 3 days, followed by slow cooling (Descent rate: 10 ℃·h^{-1}) to room temperature. Colorless block crystals of **1** were obtained. Yield: 27% (based on Mn). Anal. Calcd. for $C_{30}H_{30}MnN_4O_{14}$(%): C, 49.66; H, 4.17; N, 7.72. Found (%): C, 49.38; H, 4.24; N, 7.69. IR (KBr pellet, cm^{-1}): 3 446 (m), 3 130 (m), 1 618 (s), 1 581 (s), 1 521 (vs), 1 510 (s), 1 430 (m), 1 378 (s), 1 226 (s), 1 132 (m), 825 (m), 749 (m), 579 (w), 541 (w).

1.2.2 Synthesis of $[Zn(bbib)Cl_2]_n$ (**2**)

A mixture of bbib (0.20 mmol, 0.062 g), $ZnCl_2 \cdot 6H_2O$ (0.20 mmol, 0.049 g) was put into 6 mL H_2O and then transferred to a 25 mL Teflon-lined stainless steel vessel, heated at 110 ℃ for 3 days, followed by slow cooling (Descent rate: 10 ℃·h^{-1}) to room temperature. Colorless block crystals of **2** were obtained. Yield: 58% (based on Zn). Anal. Calcd. for $C_{20}H_{14}Cl_2N_4Zn$(%): C, 53.78; H, 3.16; N, 12.54. Found (%): C, 53.65; H, 3.23; N, 12.61. IR (KBr pellet, cm^{-1}): 3 464 (m), 1 609 (s), 1 501 (vs), 1 298 (s), 1 223 (vs), 1 119 (m), 996 (m), 826 (m), 755 (vs), 594 (w), 529 (w).

1.2.3　Synthesis of $[Zn(bbibp)Cl_2]_n$ (**3**)

The synthesis route was same with complex **2** except that bbibp replaced the bbib to react with $ZnCl_2 \cdot 6H_2O$. The orange block crystals of **3** were obtained in a yield of 43% (based on Zn). Anal. Calcd. for $C_{26}H_{18}Cl_2N_4Zn$ (%): C, 59.74; H, 3.47; N, 10.72. Found(%): C, 59.46; H, 3.54; N, 10.75. IR (KBr pellet, cm^{-1}): 3 446 (m), 1 609 (m), 1 506 (vs), 1 298 (m), 1 227 (vs), 1 119 (m), 991 (m), 902 (w), 826 (s), 755 (vs), 595 (w), 529 (w).

1.3　X-ray crystallography

Structural integrity single crystals of **1~3** were carefully selected under an optical microscope and fixed to thin glass fibers. After that, single-crystal X-ray diffraction analyses was performed on a Siemens SMART diffractometer using Mo $K\alpha$ radiation (λ = 0.071 073 nm). The structures of those titled complexes were solved by direct methods, with the non-hydrogen atoms refined anisotropially by using the SHELXTL package with F^2 values based full-matrix least-squares procedure[19]. All the hydrogen atoms except those for water molecules were generated geometrically with fixed isotropic thermal parameters, and included in the structure factor calculations[20]. And the hydrogen atoms attached to oxygen were refined with $d_{O\text{-}H}$=0.085 nm and $U_{iso,\,H}$=1.2$U_{eq,\,O}$. The crystallographic data and details of the structures for three complexes are listed in Table 1. Selected bond lengths and angles for complexes **1~3** are shown in Table S1.

CCDC: 1917435, **1**; 1917436, **2**; 1917437, **3**.

Table 1　Crystal structure parameters of complexes 1~3

Compplex	1	2	3
Empirical formula	$C_{30}H_{30}MnN_4O_{14}$	$C_{20}H_{14}Cl_2N_4Zn$	$C_{26}H_{18}Cl_2N_4Zn$
Formula weight	725.52	446.62	522.71
Temperature / K	273(2)	200(2)	200(2)
Crystal system	Monoclinic	Monoclinic	Monoclinic
Space group	*C*2/*c*	$P2_1/n$	*C*2/*c*
a / nm	1.622 96(12)	0.981 49(3)	1.292 03(4)
b / nm	1.488 01(11)	1.283 47(4)	1.519 01(4)
c / nm	1.274 25(10)	1.607 10(5)	1.116 54(3)
β / (°)	103.403(2)	105.442 0(10)	90.743 0(10)
V / nm^3	2.993 5(4)	1.951 40(10)	2.191 14(11)
Z	4	4	4
D_c / (g·cm^{-3})	1.610	1.520	1.585
F(000)	1 500	904	1 064
μ(Mo $K\alpha$) / mm^{-1}	0.523	1.544	1.388
Index ranges	−21~21, −19~19, −16~16	−12~12, −16~16, −20~20	−15~15, −18~18, −13~13
θ range for data collection / (°)	3.193~27.582	2.630~27.113	2.745~25.678
Reflection collected	23 445	34 835	15 661
Data, restraint, parameter	3 456, 4, 240	4 300, 0, 244	2 075, 0, 150
Goodness-of-fit on F^2	1.099	1.062	1.090
R_1, wR_2 [$I>2\sigma(I)$]	0.044 2, 0.108 3	0.032 1, 0.073 7	0.028 8, 0.068 1
R_1, wR_2 (all data)	0.062 3, 0.116 2	0.050 5, 0.083 8	0.038 0, 0.074 2
R_{int}	0.043 9	0.059 1	0.048 2

2 Results and discussion

2.1 Crystal structure of {[Mn(bbib)(H_2O)$_4$](H_2BTC)·2H_2O}$_n$ (1)

Structure analysis reveals that **1** is a cocrystal. Complex **1** crystallizes in the monoclinic system, space group *C*2/*c*, and its asymmetric unit consists of a half Mn(Ⅱ) ions, a half of bbib linkers, two coordinated water molecules, a half of partly deprotonated H_2BTC^{2-} anions, and one lattice water molecule (Fig. 1a). Each Mn(Ⅱ) ion locates in a distorted {MnN_2O_4} octahedral geometry, completed by two N atoms from two different bbib linkers, and four coordinated water molecules. The Mn-O/N bond lengths are in the normal range of 0.206 2(1)~0.209 0(5) nm.

The bbib linkers act as bridge when coordinating with the Mn(Ⅱ) ions, giving the 1D [Mn(bbib)]$_n$ chain with the bbib separated Mn ··· Mn distance being 1.274 3 nm (Supporting Information, Fig.S1). And the coordinated water molecules occupied other coordinated sites of Mn(Ⅱ) ions, finally giving the 1D electropositive [Mn(bbib)(H_2O)$_4$]$_n$ chain (Fig.S2). At the same time, the H_4BTC is partly deprotonated and acts as charge balances in the formation of complex **1**. Besides, the coordinated water molecules interacted with the carboxyl groups as well as the lattice water molecules through O–H ··· O hydrogen bonds, finally form the 3D supramolecular structure (Fig.1b). It is noteworthy that an unprecedented 1D water-carboxyl chain exists in the system (Fig.S3). The hydrogen bonds are given in detail in Table S2. Taking into consideration of the strong O–H ··· O hydrogen bonds, from the viewpoint of topology[21], we can define final architecture of complex **1** to be a novel 2-nodal (4,6)-connected net with the point (Schlafli) symbol of {$4^2\cdot5^8\cdot6^4\cdot7$}{$4^2\cdot6^4$} by denoting Mn(Ⅱ) ions to 6-connected nodes, the H_2BTC^{2-} anions to 4-connected nodes, respectively (Fig.1c).

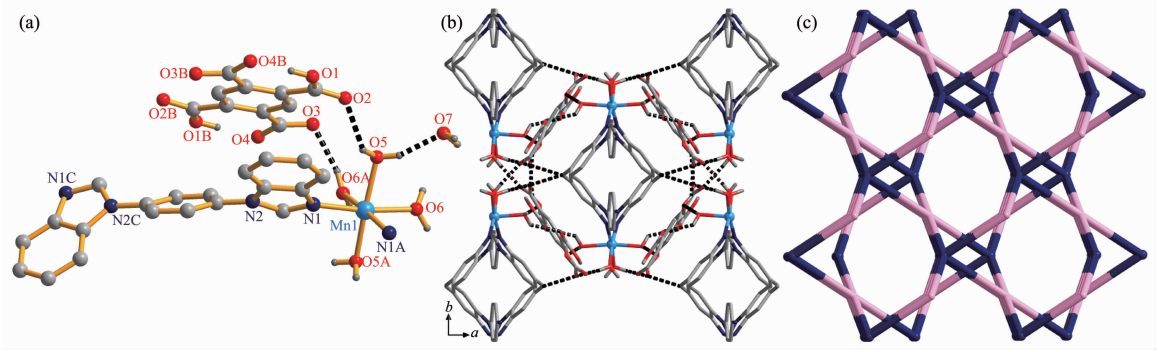

Symmetry codes: A: 1–*x*, *y*, 1/2–*z*; B: 1/2–*x*, 1/2–*y*, 1–*z*; C: 1–*x*, –*y*, 3/2–*z*

Fig.1 (a) Asymmetric unit of **1**; (b) 3D supramolecular structure of complex **1** viewed along *c* axis; (c) Schematic view of (4,6)-connected {$4^2\cdot5^8\cdot6^4\cdot7$}{$4^2\cdot6^4$} net for the architecture of **1**

2.2 Crystal structure of [Zn(bbib)Cl_2]$_n$ (2)

Complex **2** crystallizes in the monoclinic system $P2_1/n$, and the asymmetric unit contains one Zn(Ⅱ) ion, one bbib ligand, and two coordinated chloride ions (Fig.2a). The Zn(Ⅱ) ion locates in a distorted {ZnN_2Cl_2} tetrahedral geometry with the τ_4 parameter being 0.90(4) (τ_4=[360–(α+β)]/141, where α and β are the two largest bond angles in the four-coordinate complexes)[22], surrounded by two N atoms from two different bbib linkers (Zn1-N1 0.201 9(5) nm, and Zn1-N4A 0.202 1(9) nm), and two chloride ions (Zn1-Cl1 0.222 9(0) nm, and Zn1-Cl2 0.224 6(1) nm).

The bridged bbib linkers connect Zn(Ⅱ) ions to form a 1D [Zn(bbib)]$_n$ chain with the bbib separated Zn···Zn distance being 1.286 6 nm (Fig.S4), which is decorated with the chloride ions to form the 1D chain of complex **2** (Fig.S5). Furthermore, the strong C–H··· Cl hydrogen bonds (Fig.S6 and Table S3) expand these chains into a 3D architecture finally (Fig.2b). From the standpoint of topology, the final supramolecular structure of **2** can be defined as a 5-connected net with the point (Schlafli) symbol of {$4^3\cdot6^7$} by

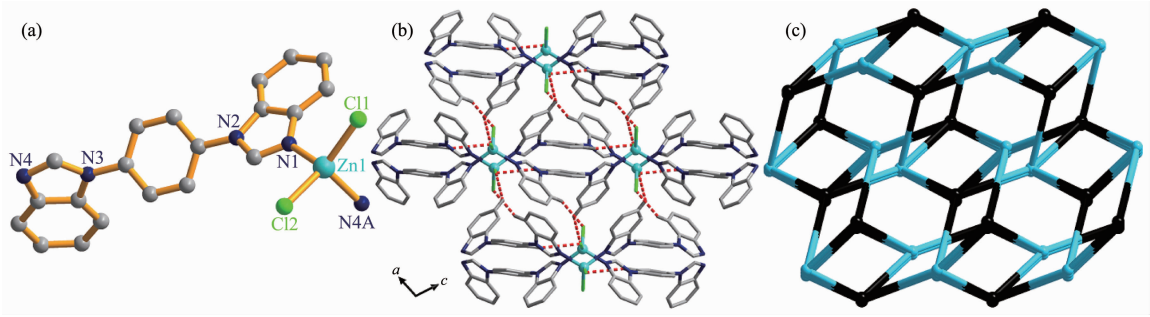

Symmetry code: A: −1/2+x, 1/2−y, 1/2+z

Fig.2　(a) Asymmetric unit of **2**; (b) Schematic view of 3D supramolecular structure of **2** along b direction; (c) Simplified 3D 5-connected $\{4^3\cdot6^7\}$ net for the architecture of **2**

denoting both the Zn(Ⅱ) ions and bbib linkers to 5-connected nodes, respectively (Fig.2c).

2.3　Crystal structure of $[Zn(bbibp)Cl_2]_n$ (3)

When the longer bbibp ligand was used to replace bbib as the bridging linker, a similar 1D chain was constructed. Complex **3** crystallizes in the monoclinic system *C*2/*c* and its asymmetric unit consists of a half of Zn(Ⅱ) ions, a half of bbibp ligands, and one chloride ion (Fig.3a). The Zn(Ⅱ) ion lies in the center of a distorted $\{ZnN_2Cl_2\}$ tetrahedral geometry with the τ_4 parameter being 0.91(3), surrounded by two N atoms from two different bbibp linkers (Zn1-N1 0.202 0(1) nm), and two chloride ions (Zn1-Cl1 0.224 0(8) nm).

The bbibp linker connected the Zn(Ⅱ) ions to form a simialr 1D $[Zn(bbibp)]_n$ chain, with the bbibp separated Zn⋯Zn distance being 1.718 6 nm (Fig.S7), which was further decorated by the chloride ions, finally leave a 1D polymeric chain of complex **3** (Fig. S8). Different from the bbib linker, the longer bbibp linker can form more C−H⋯Cl hydrogen bonds (Fig. S9 and Table S4) when interacting with adjacent chains, and finally a 3D supramolecular structure is obtained (Fig.3b). Considering the C−H⋯Cl hydrogen bonds, the 3D supramolecular structure can be simplified into a 6-connected $(4^8\cdot6^7)$-msw net by denoting the Zn(Ⅱ) ions as well as bbibp linkers to 6-connected nodes (Fig.3c).

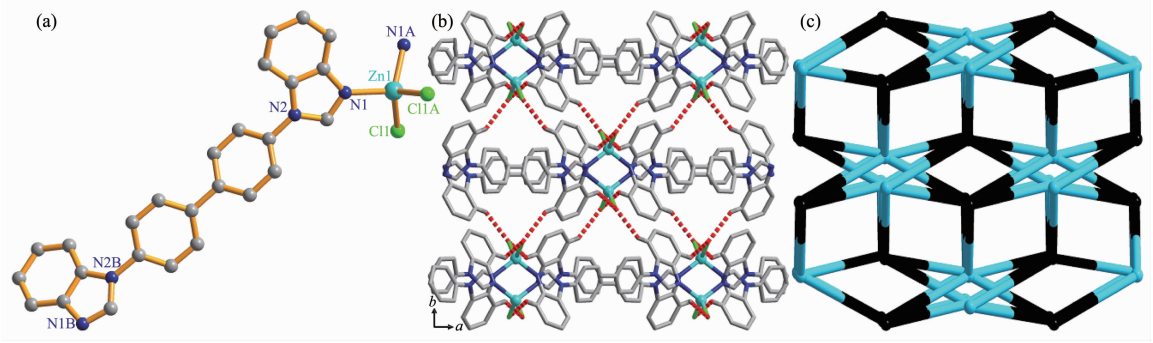

Symmetry codes: A: 1−x, y, 1/2−z; B: −x, y, 3/2−z

Fig.3　(a) Asymmetric unit of **3**; (b) Schematic view of 3D supramolecular structure of **3** along c direction; (c) Simplified 3D 6-connected $(4^8\cdot6^7)$-msw net for the network of **3**

2.4　Powder X-ray diffraction and thermogravimetric Analysis

In order to check the phase purity of those CPs, the PXRD patterns were checked and given in Fig. S10, with the peak positions of the simulated and experimental PXRD patterns are well agreed with each other, demonstrated good phase purity of those CPs. The dissimilarities in intensity may be due to the preferred orientation of the crystalline powder samples. Besides, to examine the thermal stability of these CPs, the thermogravimetric analyses were carried out from 30 to 1 000 ℃ (Fig.S11). For CP **1**, the first

weight loss of 14.47% (Calcd. 14.89%) before 110 ℃ is attributed to the loss of lattice and coordinated water molecules. And then the H_2BTC^{2-} ligands began to collapse, followed with the release of architecture. For CPs **2** and **3**, the architectures can be stable until the temperature up to about 360 ℃, and then the residual substances were decomposed gradually at above 490 ℃.

2.5 Luminescent property

The fluorescence spectra of two Zn(Ⅱ) CPs were examined in the solid state at room temperature (Fig. S12). The emission spectra exhibit strong blue-fluorescent emission peaks at 400 nm for **2**, and 402 nm for **3** with the λ_{ex}=325 nm, which can be assigned to intraligand ($\pi^*\rightarrow n$ or $\pi^*\rightarrow\pi$) emissions[23-24]. To further explore the sensing sensitivity of complexes **2** and **3** for anions, eleven kinds of solvents, including DMSO, DMF, DMA, MeCN, MeOH, EtOH, ^{n}BuOH, cyclohexanol (CXO), dioxane (DOA), H_2O, and acetone (DMK), were selected for the luminescent sensing studies to choose a suitable solvent for the detection of anions. Finely ground samples of two CPs (2 mg) were dispersed in 2 mL various solvents. As shown in Fig.4, Fig.S13 and S14, the CPs exhibit the strongest luminescence intensity in DMF for **2**, DMA for **3**, and the weakest emissions in DMK. The different intensities can be mainly attributed to the weak interactions among the solvents and the architectures of CPs[25-26]. Taking into consideration of the luminescent intensities in all solvents, especially in H_2O, as well as the actual needs of the wastewater detection, we tested the aqueous solution in the following tests. Besides, the quantum yield (Φ_f) of CPs **2** and **3** in water were tested to obtain the Φ_f being 4.7% (CP **2**) and 5.2% (CP **3**) under the excitation wavelength of 325 nm.

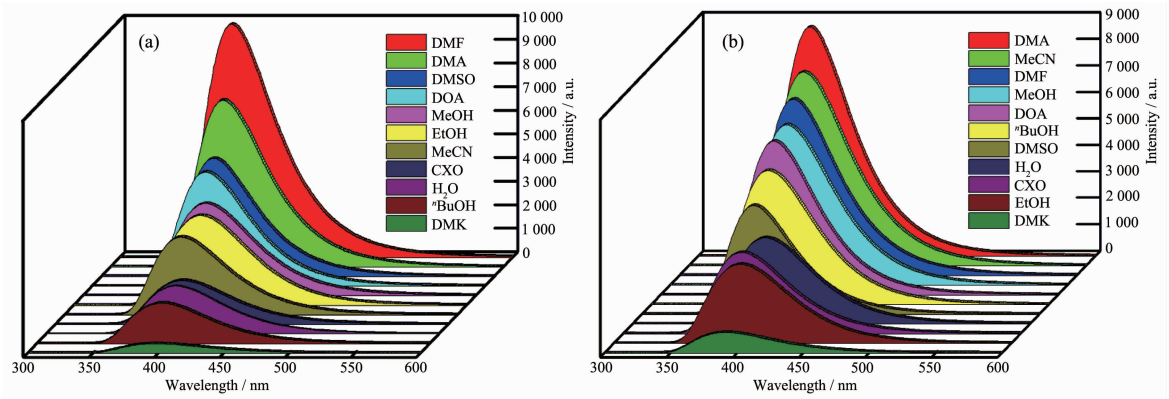

Fig.4 Luminescence intensities of CP **2** (a) and **3** (b) dispersed in different solvents

2.6 Luminescent sensing

The investigation of selectivity of the sensing ability for various anions were performed by adding 2 mg finely ground samples of the CPs into 2 mL of 0.01 mol·L^{-1} aqueous solutions of twelve metal ions (K^+, Na^+, Ag^+, Ca^{2+}, Ba^{2+}, Cu^{2+}, Co^{2+}, Zn^{2+}, Cd^{2+}, Fe^{2+}, Al^{3+}, and Fe^{3+}) at room temperature. As can be seen in the Fig.5a, 5b, S15 and S16, the luminescence intensity of M^{n+}@CPs suspensions were heavily dependent on the species of metal ions. And the Fe^{3+} exhibited extremely significant luminescent quenching effects.

To better understand the luminescence responses of the CPs to Fe^{3+} ions, the relationships between the concentrations of Fe^{3+} ions and the luminescence intensities were studied. As shown in Fig.5c and 5d, with increasing addition of Fe^{3+} ions, the intensities of luminescence were steadily decreased with the quenching rates increasing (Fig.S17). In the concentration range from 0 to 0.25 mmol·L^{-1}, the plots of I_0/I (I_0 and I are the luminescence intensities of the emulsions in the absence and presence of Fe^{3+} ions) vs the concentrations of Fe^{3+} ions are given in Fig.5e and 5f. For CPs **2** and **3**, the I_0/I vs the concentrations of Fe^{3+} ions can be well-fit to the equations of I_0/I= 2.07exp(3 134$c_{Fe^{3+}}$)−1.02 (R=0.999 08) with the K_{sv} being 9 800 L·mol^{-1}, and the Stern-Volmer equation of I_0/I=5 430$c_{Fe^{3+}}$+1.00 (R=0.997 93), respectively[27-28].

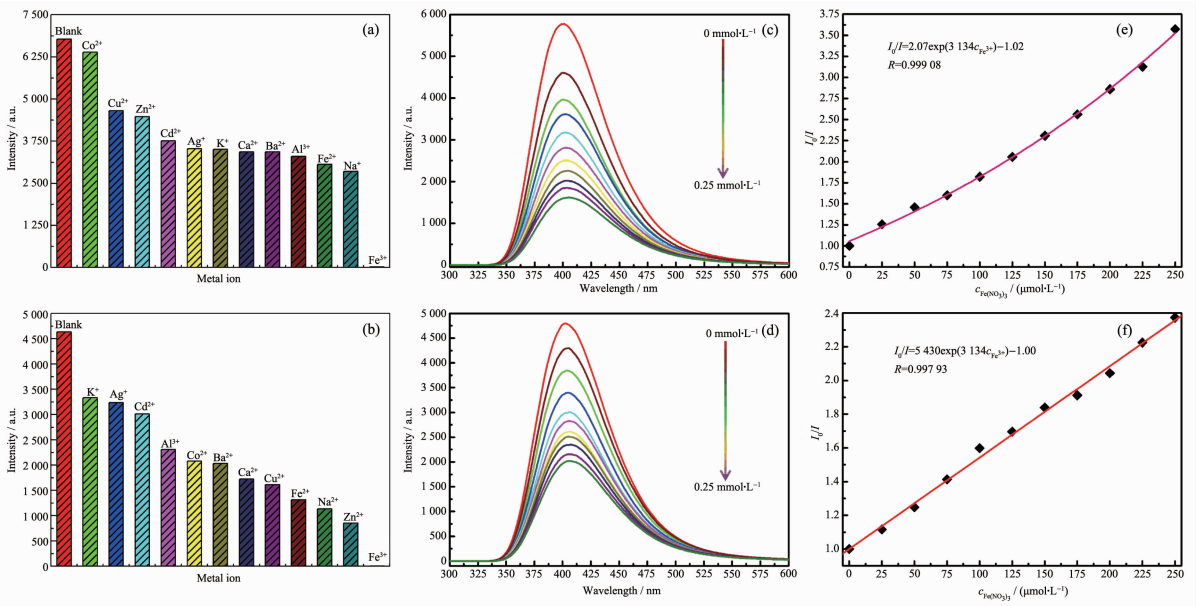

Fig.5　Luminescence intensities of CP **2** (a) and **3** (b) dispersed in aqueous solution of different anions; Effect on the emission spectra of CP **2** (c) and **3** (d) dispersed in aqueous solutions upon incremental addition of $Fe(NO_3)_3$; I_0/I vs concentration of $Fe(NO_3)_3$ with CP **2** (e) and **3** (f) as sensors

The detection limit calculated by $3\sigma/K_{SV}$ (σ is the standard deviation for ten cycles of luminescence tests using the blank solution at room temperature) presented the low value of 0.869 4 μmol·L^{-1} for CP **2**, and 1.569 μmol·L^{-1} for CP **3**. To verify the repeatability as well as the PL intensity stable in aqueous system of the CPs as sensors in sensing of Fe^{3+}, three recycled tests were given, which indicates stable PL intensity and good repeatability (Fig.S18). After three recycled tests, the PXRD patterns of two complexes are still well correspond with the simulated ones (Fig.S19), indicating that the stability of the CPs as sensors to detect Fe^{3+} ions in aqueous solution[29-30].

The possible luminescence quenching mechanism of Fe^{3+} for the CPs was investigated. As proved by the PXRD, the architectures of the CPs are stable, which indicating the luminescence quenching was not caused by the structure collapse. The UV-Vis absorption spectra of $Fe(NO_3)_3$, CPs **2** and **3** in aqueous solution were recorded and given in Fig.S20. The UV-Vis absorption spectrum of $Fe(NO_3)_3$ in aqueous solution showed broad absorption bands at 240~400 nm, which covered the absorption bands of the the CPs, indicating that there are competitive absorptions of the exciting light between the Fe^{3+} and the CPs. Hence, the luminescence quenching may be the process involving competitive absorption on light excitation between the Fe^{3+} ions and the architecture of the CPs.

3　Conclusions

Three 1D coordination polymers were constructed from the solvothermal reaction of bis(benzimidazo-1-ly) linkers (bbib and bbibp) and transition metal salts, with the final packing architectures being (4,6)-connected $\{4^2\cdot5^8\cdot6^4\cdot7\}\{4^2\cdot6^4\}$ net for **1**, 5-connected $\{4^3\cdot6^7\}$ net for **2**, and 6-connected $(4^8\cdot6^7)$-msw net for **3**, respectively. Structural analysis reveals that the strong O–H⋯O hydrogen bonds in **1**, and C–H⋯Cl hydrogen bonds in **2** and **3** play important roles in the formation of 3D structures of these complexes. Besides, the luminescent sensing investigation indicates that CPs **2** and **3** exhibit highly sensitivity and selectively sensing for Fe^{3+} ion in aqueous solution.

Supporting information is available at http://www.wjhxxb.cn

References:

[1] Pan M, Zhu Y X, Wu K, et al. *Angew. Chem. Int. Ed.*, **2017**, **56**(46):14582-14586

[2] Fan L, Fan W, Li B, et al. *CrystEngComm*, **2015**,**17** (25):

4669-4679

[3] Zhao D, Li X H, Guo J H, et al. *Inorg. Chem.*, **2018**,**57**(5): 2695-2704

[4] Zhang S S, Alkan F, Su H F, et al. *J. Am. Chem. Soc.*, **2019**, **141**(10):4460-4467

[5] Jiang J C, Zhao Y B, Yaghi O M. *J. Am. Chem. Soc.*, **2016**, **138**(10):3255-3265

[6] Chen Y J, Wang R, Wang S, et al. *Chem. Commun.*, **2018**, **54**(96):13563-13566

[7] Fan L, Fan W, Li B, et al. *Dalton Trans.*, **2015**,**44**(5):2380-2389

[8] ZHAI Li-Jun(翟丽军), NIU Yu-Lan(牛宇岚), HAO Xiao-Yan (郝小燕), et al. *Chinese J. Inorg. Chem.*(无机化学学报), **2018**,**34**(10):1936-1942

[9] Fan L M, Zhang X T, Li D, et al. *CrystEngComm*, **2013**,**15** (2):349-355

[10]Liu J W, Wang Z, Chai Y M, et al. *Angew. Chem. Int. Ed.*, **2019**,**58**(19):6276-6279

[11]Yang X G, Ma L F, Yan D P, et al. *Chem. Sci.*, **2019**,**10** (17):4567-4572

[12]Fan L, Zhao L, Wang J, et al. *J. Solid State Chem.*, **2018**, **266**:189-195

[13]Zhang X T, Chen H T, Li B, et al. *Dalton Trans.*, **2018**,**47** (4):1202-1213

[14]Chen L, Zhou J, Cui H H, et al. *Dalton Trans.*, **2018**,**47**(8): 2506-2510

[15]Wang Z, Sun H T, Kurmoo M, et al. *Chem. Sci.*, **2019**,**10** (18):4862-4867

[16]Zhang Y, Gao L, Zhang J, et al. *J. Solid State Chem.*, **2019**, **271**:40-46

[17]Fan L, Gao L, Ren G, et al. *J. Solid State Chem.*, **2018**,**264**: 15-21

[18]Zhao Y, Yang X G, Lu X M, et al. *Inorg. Chem.*, **2019**,**58** (9):6215-6221

[19]Sheldrick G M. *SHELXS*-97, *Program for Crystal Structure Refinement*, University of Göttingen, Germany, **1997**.

[20]Sheldrick G M. *SHELXL*-97, *Program for Crystal Structure Solution*, University of Göttingen, Germany, **1997**.

[21]Blatov V A. *Struct. Chem.*, **2012**,**23**(4):955-963

[22]Yang L, Powell D R, Houser R P. *Dalton Trans.*, **2007**(9): 955-964

[23]Fan L M, Fan W L, Li B, et al. *CrystEngComm*, **2015**,**17** (48):9413-9422

[24]Fan L, Wang X, Zhang Y, et al. *Z. Anorg. Allg. Chem.*, **2017**,**643**(24):2138-2143

[25]Zhang J, Gao L, Wang Y, et al. *New J. Chem.*, **2019**,**43**(24): 9376-9383

[26]Zhang J, Huo L, Wang X, et al. *Cryst. Growth Des.*, **2017**,**17** (11):5887-5897

[27]Fan L, Zhang Y, Liang J, et al. *CrystEngComm*, **2018**,**20**(33): 4752-4762

[28]Yan X, Ma L F, Yan D. *Chem. Sci.*, **2019**,**10**(17):4567-4572

[29]Wang J, Gao L, Zhang J, et al. *Cryst. Growth Des.*, **2019**,**19** (2):630-637

[30]Fan L, Zhang Y, Wang J, et al. *J. Solid State Chem.*, **2018**, **260**:46-51